

# Observation of two species of vortices in the anisotropic spin-triplet superconductor $\text{Sr}_2\text{RuO}_4$

V.O. Dolocan <sup>\*,1</sup> P. Lejay,<sup>1</sup> D. Mailly,<sup>2</sup> and K. Hasselbach<sup>1</sup>

<sup>1</sup>*CRTBT-CNRS, 25 Avenue des Martyrs, 38042 Grenoble, France*

<sup>2</sup>*LPN-CNRS, Route de Nozay, 91460 Marcoussis, France*

(Dated: March 23, 2022)

## Abstract

Magnetic flux structures in single crystals of the layered spin triplet superconductor  $\text{Sr}_2\text{RuO}_4$  are studied by scanning micro SQUID Force microscopy. Vortex chains appear as the applied field is tilted along the in-plane direction of the superconductor. The vortex chains align along the direction of the in-plane component of the applied magnetic field. The decoration of in-plane vortices by crossing Abrikosov vortices is observed: two vortex orientations are apparent simultaneously, one along the layers and the other perpendicular to the layers. The crossing vortices appear preferentially on the in-plane vortices.

PACS numbers: 74.20.Rp, 74.25.Qt, 74.70.Pq, 85.25.Dq

---

\* Present address: Max Plank Institute for Chemical Physics of Solids, 40 Nöthnitzer Str., 01187 Dresden, Germany

## I. INTRODUCTION

The magnetic properties of superconductors depend strongly on their crystalline and electronic anisotropy. Prominent examples are the high temperature superconductors. Intense research efforts have revealed a variety of vortex phenomena in these compounds (vortex-glass, vortex melting, crossing of Josephson and pancake vortices). The general theoretical approach on vortex matter is based on the anisotropic Ginzburg-Landau (GL) theory. There the anisotropy is expressed in terms of the effective mass of the electron. For layered anisotropic superconductors, the out of plane effective mass,  $m_c$ , is much larger than the in plane effective masses ( $m_c \gg m_{ab}$ ). To describe this anisotropy the parameter  $\gamma = (m_c/m_{ab})^{1/2} = \lambda_c/\lambda_{ab}$ [1] is used. For example in NbSe<sub>2</sub>  $\gamma=3.3$ , in YBCO  $\gamma=5-8$  and in BSCCO  $\gamma$  is higher than 150,  $\gamma$  being dependent on the oxygen doping of the high  $T_c$  superconductors.

In moderately anisotropic superconductors, when the magnetic field is tilted away from the anisotropy axis, calculations based on GL theory show that the screening currents tend to flow in approximately elliptical paths around the vortex cores and parallel to the layers[2, 3]. This current flow creates a net transverse magnetization and attraction appears between the tilted vortices, leading finally to the development of vortex chains, formed by inclined vortices. These vortex chains have been observed in YBCO[4].

In highly anisotropic superconductors, Josephson vortices appear if the distance between the layers is larger than  $\xi_c$ . The Josephson vortices are confined in the space between the layers. The Lawrence-Doniach (LD) model is used as the continuous GL theory cannot be applied anymore. In the LD model the tilted vortex is described as tilted stack of 2D pancake vortices connected by Josephson strings. Pancake vortices are characterized by circular supercurrent pattern flowing in the layers and Josephson strings being short segments of Josephson vortices confined to the insulating region between the superconducting layers. High  $T_c$  superconductors with a weak interlayer coupling, like BSCCO, are treated as 2D superconductors according to the Lawrence-Doniach model. Magnetic imaging of vortices was quintessential for the experimental exploration of vortex structures in BSCCO: Bitter decoration experiments revealed vortex chains separated by a vortex lattice[5], scanning Hall probe microscopy showed Josephson vortices decorated by pancake vortices[6, 7].

In the present study vortex matter is investigated in the anisotropic layered supercon-

ductor  $\text{Sr}_2\text{RuO}_4$ . The superconducting transition temperature of  $\text{Sr}_2\text{RuO}_4$  is of the order of 1.45 K[8]. Like high  $T_c$  cuprates, the tetragonal  $\text{Sr}_2\text{RuO}_4$  has a layered structure, the  $\text{RuO}_2$  planes are separated by 12.74 Å and has highly anisotropic properties[9].  $\text{Sr}_2\text{RuO}_4$  has a  $\gamma$  value of 20 situating it between YBCO and BSCCO on the anisotropy scale. We expect  $\text{Sr}_2\text{RuO}_4$  to act more like a 3D superconductor as the c-axis parameter is 3 times smaller than the coherence length  $\xi_c$ . The Ginzburg-Landau parameter  $\kappa = \lambda/\xi$  is around 2.3 when the magnetic field is applied along the c-axis direction and 46 for the in-plane direction. The physical properties of  $\text{Sr}_2\text{RuO}_4$  are very rich and indications accumulated that it might exhibit unconventional superconductivity[10, 11, 12]. A coherent picture can be obtained in terms of a superconducting state characterized by breaking of time reversal symmetry and requiring a multi-component order parameter of p-wave symmetry with a gap function  $d=\hat{z}(k_x \pm ik_y)$ . The symmetry of the order parameter should give rise to domains of opposite chirality,  $\hat{z}(k_x + ik_y)$  and  $\hat{z}(k_x - ik_y)$ , separated by domain walls, formation of fractional vortices on the domain walls and should generate spontaneous currents at the edges of the crystal. It was conjectured that domain walls might be preferential pinning sites for vortices[13]. Magnetic microscopy is a means of choice to study the relevance of these predictions. Vortices along with vortex coalescence were observed in  $\text{Sr}_2\text{RuO}_4$  by  $\mu\text{SQUID}$  magnetic microscopy [14]. Here we focus on vortex matter in  $\text{Sr}_2\text{RuO}_4$ , demonstrating the presence of tilted vortex chains in, and evidencing pinning of perpendicular vortices on in-plane vortex chains in  $\text{Sr}_2\text{RuO}_4$ , making  $\text{Sr}_2\text{RuO}_4$  the first anisotropic 3D superconductor presenting crossing vortices.

We use for magnetic imaging a high resolution scanning  $\mu\text{SQUID}$  microscope ( $S\mu\text{SM}$ )[15] working in a dilution refrigerator. The  $S\mu\text{SM}$  has an aluminum  $\mu\text{SQUID}$  as pickup loop of 1.2 $\mu\text{m}$  diameter. The critical current of the  $\mu\text{SQUID}$  is a periodic function of the magnetic flux emerging perpendicularly from the sample surface. The images shown are maps of the critical current value of the  $\mu\text{SQUID}$  scanning the surface. We used two different high quality crystals coming from the same rod showing volume superconductivity below a temperature of 1.31K. The two samples are large plates with thickness of 0.5mm and 0.6mm. The surface is cleaved and AFM images show flatness down to the order of 6 Å. The magnetic fields are applied by a solenoid and a rotatable Helmholtz coil, the coils are at room temperature. The solenoid axis is parallel to the ab face of the sample ( $H_a$  in the Fig. 1e) and the Helmholtz coil generates a field, ( $H_{bc}$ ), perpendicular to the solenoid axis. Adjusting the relative angle

and the magnitude of the two fields allow us to point the resultant field along any direction.

## II. VORTEX CHAINS IN $\text{Sr}_2\text{RuO}_4$

Vortex chains form in  $\text{Sr}_2\text{RuO}_4$  [16] at low fields and tilt angles higher than  $70^\circ$  from c-axis. In Fig. 1 only a field  $H_{bc}$  was applied at an angle  $\varphi$  of  $87^\circ$  from c axis and the magnetic flux was increased from 0 to 70 gauss. Each measurement was acquired after a field cooling procedure. The vortex chains start to appear in our images for fields higher than 20 gauss,  $2H_{c1}$  for the in-plane direction of our sample. As the field is increased the chain density increases also. When the number of vortices reaches an equilibrium value in each chain the formation of a new chain becomes energetically favorable.

Calculations in the GL theory in the London limit[17] show that the intra-chain distance between vortices remains constant with increasing field while the inter-chain distance decreases like  $B^{-1}$ . This distance can be calculated in the single chain limit and, using the parameters of  $\text{Sr}_2\text{RuO}_4$ , the vortex vortex intra-chain distance yields  $2\lambda_{ab} \sim 0.3\mu\text{m}$ , lower than our SQUID resolution. On the other hand we can measure the inter-chain distance between the chains and compare it with the GL theory. In our experiment on  $\text{Sr}_2\text{RuO}_4$ , at low perpendicular fields the distance between the chains follows the  $B^{-1}$  dependence as in the GL theory (Fig. 1f, fitted points), though the value of the observed spacing is larger than predicted. As the field increases the distance between the chains should tend monotonously to the isotropic limit (the line,  $B^{-1/2}$  dependence). A regular square lattice is observed by SANS for fields higher than 50G applied along the c-axis. With increasing perpendicular field, we observe that the inter-chain distance deviates from the  $B^{-1}$  dependence characteristic of vortex chains (Fig. 1f, points not fitted). The chains seem to accommodate a higher density of vortices than predicted by the London theory, retarding the formation of the vortex lattice. This finding is consistent with vortex coalescence [14] in  $\text{Sr}_2\text{RuO}_4$  at intermediate magnetic fields applied parallel to c-axis.

Ginzburg-Landau theory predicts that the vortex chains are aligned in the plane spanned by the crystal's anisotropy axis and the applied field. When the applied field is rotated in the ab-plane, the vortex chains should follow. We undertook these measurements on the second crystal, in turning the in-plane component of the field vector by an angle  $\alpha$  relative to the bc-plane. The field was applied in superposing two fields:  $H_a$  oriented along a-axis,

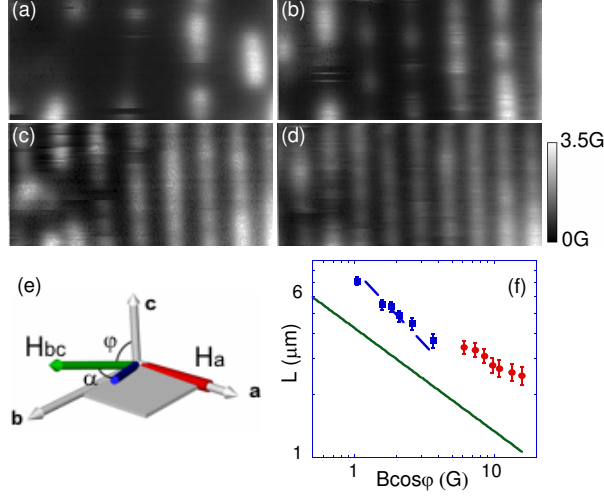


FIG. 1: (Color online) Scanning  $\mu$ SQUID microscope images of the magnetic flux above the ab-face of  $\text{Sr}_2\text{RuO}_4$  at  $T=0.35\text{K}$ . During field cooling the magnetic field is applied at a fixed angle  $\varphi=87^\circ$  from c-axis varying for each panel as: (a) 20 G, (b) 35 G, (c) 60 G and (d) 70 G. The image area is  $31\mu\text{m}\times 15\mu\text{m}$ . The magnetic scale is shown on the right. (e) Scheme of the 2 applied magnetic fields. The magnetic field  $H_{bc}$  can be rotated with an angle  $\varphi$  from the c-axis (in the bc-plane). A second fixed magnetic field  $H_a$  can be applied in-plane. The resultant field is also shown schematically. (f) Inter-chain distance as function of normal field. The points are fitted with a  $B^{-1}$  law. The line represents the isotropic limit ( $B^{-1/2}$ ).

and the field in the bc-plane  $H_{bc}$  tilted from the c-axis by the angle  $\varphi$ . Each measurement was done after field cooling (Fig. 2). We varied the direction  $\alpha$  of the in-plane component from  $0^\circ$  to  $90^\circ$ . The linear vortex chains align with the in-plane direction of the applied field as expected. The features in the magnetic images that are fixed are due to flux pinned at surface asperities. In the panel a) the broadened flux lines are attributed to the simultaneous presence of vortex chains and vortex coalescence, fostered by a perpendicular field of 9 G. For some values of the perpendicular field the vortices in chains are well separated like in the image c) when the perpendicular field is of the order of 3.5 G. These single vortices seem to be pinned on the vortex chains, reminiscent of decoration of Josephson vortices by pancake vortices observed in the 2D superconductor BSCCO. Exploring the history dependence of the magnetic field penetration in the crystal allows us to examine this novel state in the anisotropic 3D superconductor in more detail.

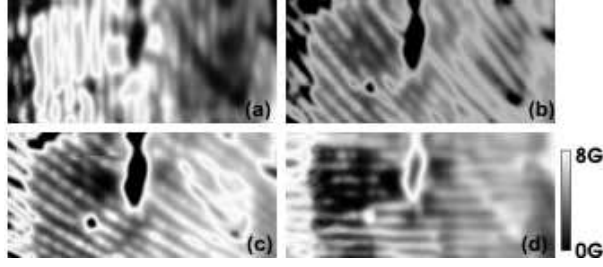


FIG. 2: Rotation of vortex chains in  $\text{Sr}_2\text{RuO}_4$ . When the amplitudes of the two different magnetic fields are varied the angle  $\alpha$  of the resultant field is changed: (a)  $H_{bc}=54\text{G}$ ,  $\varphi=80^\circ$ ,  $\alpha=0^\circ$ ; (b)  $H_{bc}=54\text{G}$ ,  $H_a=54\text{G}$ ,  $\varphi=85^\circ$ ,  $\alpha=45^\circ$ ; (c)  $H_{bc}=39.3\text{G}$ ,  $H_a=68\text{G}$ ,  $\varphi=85^\circ$ ,  $\alpha=60^\circ$ ; (d)  $H_{bc}=-6\text{G}$ ,  $H_a=90\text{G}$ ,  $\varphi=0^\circ$ ,  $\alpha=90^\circ$ . All images are taken after field cooling at a temperature of  $0.6\text{K}$ . The dimensions of each image are  $62\mu\text{m}\times 30\mu\text{m}$ .

### III. CROSSING VORTICES IN $\text{Sr}_2\text{RuO}_4$

In order to explore the vortex pinning and the vortex chain mechanism in  $\text{Sr}_2\text{RuO}_4$  we undertook measurements changing the applied magnetic field while the sample is in the superconducting state. The magnetic field component parallel to the plane is higher than the first critical field  $H_{c1}$  in the in-plane direction ( $H_{c1}^{ab}=10\text{G}$ ), while the perpendicular component is lower than  $H_{c1}$  ( $H_{c1}^c=50\text{G}$ ). In a first approximation a formation of tilted vortex chains might be expected as shown in the field cooled case (see Fig. 1). With magnetic fields close to the ab-plane for different field preparations we observe vortices decorating flux channels. We observe also a tendency for a long-range anticorrelation between decorating vortices in adjacent chains reminding a distorted hexagonal lattice. This anticorrelation may be a sign that the vortex pinning on the chains is weak. Zero field cooling (ZFC) Fig. 3(a)-(c) and field cooling (FC) Fig. 1c) sample preparation result in different vortex configurations: we observe the decoration of flux channels mostly in the ZFC experiments. Due to the lower first critical field the magnetic flux penetrates preferentially along the planes, forming the flux channels, and the perpendicular vortices are pinned on the flux channels. In the FC experiments for a wide range of angles the flux expulsion happens in such a way that only tilted vortices appear in the sample. In Fig. 2(c) aligned vortices can be seen. The distinction of chains of tilted vortices and flux channels along the planes is made considering the amplitude of the signal. As shown by the magnetic scales on the right of each image in Fig. 3, in the (a)-(c) images the vortices have a similar magnetic amplitude as the vortices

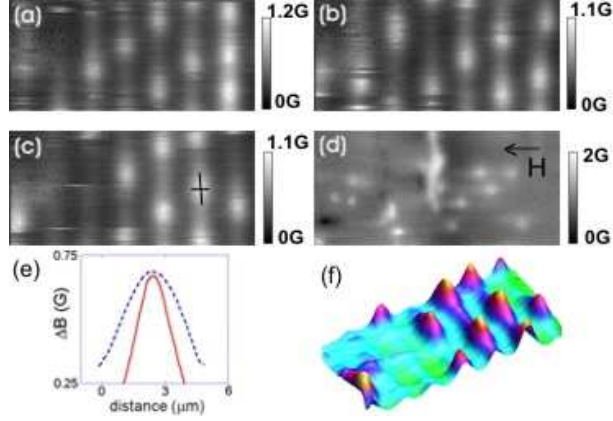


FIG. 3: (Color online) Crossing vortices in  $\text{Sr}_2\text{RuO}_4$ . The (a)-(c) images are taken after different field preparations: (a) 50 G ZFC, (b) 5 G FC and increased to 50 G at low temperature, (c) 10 G FC and increased to 50 G at low T. The magnetic scale for each image is shown on the right. The dimensions are  $31\mu\text{m} \times 15\mu\text{m}$  and the imaging temperature is 0.35K. The tilting angle is  $87^\circ$ . (d) 68G FC with field applied only in plane (indicated by an arrow). An 'halo' around each perpendicular vortex is visible. The dimensions of the image are  $62\mu\text{m} \times 30\mu\text{m}$ . (e) Two perpendicular line scans at one of the decorating vortices (indicated by a cross in panel c). The image (f), is the 3D representation of the image (c).

present when the field is applied along the c-axis[14]. A normal component of the field of the order of 0.4 Gauss creates these vortices. In the FC case (Fig. 1c) the magnetic flux coming out of the sample has much larger amplitude as if the vortices would be closer together. We should have around 70 vortices in the image for the FC case but the vortices appear as tilted vortices forming a vortex chain. All the images in Fig. 1 and Fig. 3(a)-(c) are taken at the same place of the sample. We observe also that the decorating vortices have oval shape (Fig. 3d), similar to the pancake vortices decorating Josephson vortices[18]. In the case of BSCCO the deformation is explained by a displacement of the pancake vortices due to circulating currents of the Josephson vortices[19]. In a similar manner the interaction between in-plane flux channels and the crossing vortices may result in the elongated shape of the decorating vortices detected by the SQUID. The perpendicular vortices appear due to a small residual field estimated to be 0.15G. The deformation of the vortex shape is a sign for the strong interaction between the two species of vortices and confirms the finding that the crossing vortices are pinned on the flux channels running along the layers.

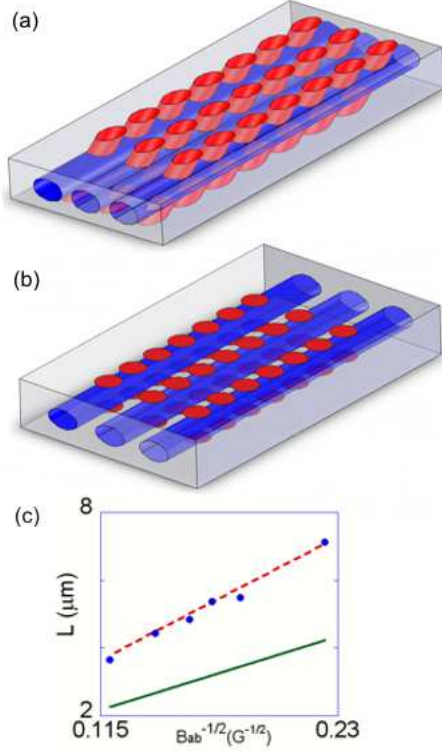


FIG. 4: (Color online) Scheme of interpenetrating vortices: (a)tilted vortices and (b)pancake vortices crossing Josephson vortices. (c)the inter-chain distance as function of the in plane component of the field  $B_{ab}^{-1/2}$ , supposing the applicability of the Lawrence Doniach model. The dashed line represents the theoretical values of the inter-chain distance calculated from eq.1 with  $\gamma=28$ . The line represents the values calculated with  $\gamma=20$ .

#### IV. DISCUSSION

In isotropic superconductors at low tilted fields the flux lines penetrate parallel to each other and with the average field in the sample and arrange in a pattern that minimizes the interaction energy. If the superconductor is strongly anisotropic the free energy of the vortex state has two local minima and consequently a flux line can penetrate in two distinct directions in the material. For high anisotropy only flux lines that are nearly parallel or perpendicular to the layers are stable[20, 21]. In the LD model this corresponds to the separation in pancake vortices and Josephson vortices. The distance between the Josephson vortices is given by[19]  $L = \sqrt{\sqrt{3}\gamma\phi_0/(2B_{ab})}$  (1), where  $B_{ab}$  is the in plane field (parallel field) and  $\phi_0$  is the quantum of flux. In  $\text{Sr}_2\text{RuO}_4$  this distance should correspond to the inter-chain distance supposing the LD model applies. In the Fig 4c) the inter-chain distance is



shown function of  $B_{ab}^{-1/2}$ . The dashed line passing through the measured points represents the theoretical values calculated with the formula (1) for an anisotropy parameter  $\gamma=28$ . The line represents the theoretical calculation for a  $\gamma=20$ , which corresponds to the values found in the literature[9]. The anisotropy parameter  $\gamma$  is determined from the ratio of the critical fields or penetration depths. A value of 15-20 was found also by  $\mu$ SQUID microscopy, imaging the ac face of the crystal and determining the deformation of the vortex (images not shown). As the superconductivity is thought to be orbital dependent[22], the anisotropy parameter could vary (giving rise to two different penetration depths) and an anisotropy parameter value of 28 might be plausible. The structures observed would then correspond to pancake vortices pinned on Josephson vortices (Fig. 4b). However,  $\text{Sr}_2\text{RuO}_4$  should act more like a 3D superconductor as the coherence length is three times longer than the interlayer spacing. This makes the observed decoration of in-plane flux channels by crossing vortices unique.

The presence of Josephson vortices is not a necessary prerequisite for the presence of crossing vortices: in the classical London theory two parallel vortices repel each other. This repulsion is maintained if one tilts one of the vortices from the common direction. The interaction energy is given by:  $E_{int} = \frac{\phi_0^2}{2\mu_0\lambda_{ab}} \cot(\alpha) \exp(-\frac{d}{\lambda_{ab}})$  where  $d$  is the smallest distance between vortices and  $\alpha$  the angle between them[23]. When the angle between vortices becomes  $90^\circ$  the flux lines do not interact. If the angle increases more the flux lines start to attract each other and the highest attraction energy is for the antiparallel direction. Daemen *et al.*[24] showed that the free energy of a mixed lattice formed by vortices parallel to the c axis and vortices inclined at some angle from the c axis is lower than the free energy of a deformed inclined lattice. This model predicted that two types of vortices may be observed in  $\text{Sr}_2\text{RuO}_4$ , formed by two interpenetrating lattices (Fig. 4a), a lattice of vortices parallel to the layers and decorating vortices that are nearly parallel to the c-axis.

## V. CONCLUSION

We imaged two types of vortex configurations in the anisotropic spin triplet superconductor  $\text{Sr}_2\text{RuO}_4$ . The first configuration are vortex chains formed by tilted vortices. The qualitative variation of the vortex chain spacing is consistent with GL theory though the vortex spacing is closer than predicted. For higher perpendicular fields we see that the

variation of the vortex chain spacing is slower than predicted, resulting in a higher vortex density in the chain. This accommodation of a higher vortex density may be related to the observed vortex coalescence in  $\text{Sr}_2\text{RuO}_4$ .

The second vortex configuration consists of in-plane flux channels crossed by perpendicular Abrikosov vortices. The observed deformation of the pinned Abrikosov vortices is a sign for the interaction between the Abrikosov vortices and the flux channels. The strong inter-layer coupling of  $\text{Sr}_2\text{RuO}_4$  excludes the existence of Josephson vortices in this compound, precluding the applicability of the Lawrence Doniach model of an interplay between Josephson vortices and pancake vortices, well established for crossing vortices observed in high  $T_c$  superconductors. The possibility of crossing vortices is predicted in the case of sufficiently anisotropic 3D superconductors, we think that this is the case here. Our observations are qualitatively understood, for a more quantitative interpretation the theoretical models have yet to be developed taking into account the physical properties of  $\text{Sr}_2\text{RuO}_4$ , quite different from those of other anisotropic superconductors. We are shedding light on aspects of vortex physics in exploring vortex chain formation and of flux channels decorated by vortices and in particular we show the richness of physical phenomena in  $\text{Sr}_2\text{RuO}_4$ .  $\text{Sr}_2\text{RuO}_4$  is at the intersection of many different domains: unconventional superconductivity, anisotropy and nonlocal electrodynamics of low  $\kappa$  superconductors.

## Acknowledgments

We acknowledge the support of CNRS, and fruitful discussions with Y. Liu, P. Rodière and T. Prouvé.

- 
- [1] J. R. Clem, Super. Sci. Tech. **11**, 909 (1998).
  - [2] A. I. Buzdin and A. Yu. Simonov, Zh. Eksp. Teor. Fiz. **98**, 2074 (1990) [Sov. Phys. JETP **71**, 1165 (1990)].
  - [3] V. G. Kogan, Phys. Rev. B **24**, 1572 (1981).
  - [4] P. L. Gammel, D. J. Bishop, J. P. Rice, and D. M. Ginsberg, Phys. Rev. Lett. **68**, 3343 (1992).
  - [5] C. A. Bolle, P. L. Gammel, D. G. Grier, C. A. Murray, D. J. Bishop, D. B. Mitzi and A. Kapitulnik, Phys. Rev. Lett. **66**, 112 (1991).

- [6] A. Grigorenko, S. Bending, T. Tamegai, S. Ooi and M. Henini, *Nature(London)* **414**, 728 (2001).
- [7] S. J. Bending and M. J. W. Dodgson, *J. Phys. Cond. Mat.* **17**, R955, (2005).
- [8] Y. Maeno, H. Hashimoto, K. Ioshida, S. Nishizaki, T. Fujita, J. Bednorz and F. Lichtenberg, *Nature(London)* **372**, 532 (1994).
- [9] A. P. Mackenzie and Y. Maeno, *Rev. Mod. Phys* **75**, 657 (2003).
- [10] K. Ishida, H. Mukuda, Y. Kitaoka, K. Asayama, Z. Q. Mao, Y. Mori and Y. Maeno, *Nature(London)* **396**, 658 (1998).
- [11] K. D. Nelson, Z. Q. Mao, Y. Maeno and Y. Liu, *Science* **306**, 1151 (2004).
- [12] G. M. Luke, Y. Fudamoto, K. M. Kojima, M. I. Larkin, J. Merrin, B. Nachumi, Y. J. Uemura, Y. Maeno, Z. Q. Mao, Y. Mori, H. Nakamura and M. Sgrist, *Nature(London)* **394**, 558 (1998).
- [13] M. Sgrist and D. F. Agterberg, *Prog. Theor. Phys.* **102**, 965 (1999).
- [14] V. O. Dolocan, C. Veauvy, F. Servant, P. Lejay, K. Hasselbach, Y. Liu and D. Mailly, *Phys. Rev. Lett.* **95**, 097004 (2005).
- [15] C. Veauvy, D. Mailly, and K. Hasselbach, *Rev. Sci. Instr.* **73**, 3825 (2002).
- [16] V. O. Dolocan, C. Veauvy, Y. Liu, F. Servant, P. Lejay, K. Hasselbach and D. Mailly, *Physica C* **404**, 140 (2004).
- [17] L. L. Daemen and L. J. Campbell and V. G. Kogan, *Phys. Rev. B* **46**, 3631 (1992).
- [18] A. N. Grigorenko, S. J. Bending, I. V. Grigorieva, A. E. Koshelev, T. Tamegai and S. Ooi, *Phys. Rev. Lett.* **94**, 067001 (2005).
- [19] A. E. Koshelev, *Phys. Rev. Lett.* **83**, 187 (1999).
- [20] D. A. Huse, *Phys. Rev. B* **46**, 8621 (1992).
- [21] A. Sudbo, E. H. Brandt and D. A. Huse, *Phys. Rev. Lett.* **71**, 1451 (1993).
- [22] D. F. Agterberg and T. M. Rice and M. Sgrist, *Phys. Rev. Lett.* **78**, 3374 (1997).
- [23] A. Sudbo, E. H. Brandt, *Phys. Rev. Lett.* **67**, 3176 (1991).
- [24] L. L. Daemen and L. J. Campbell and A. Yu. Simonov and V. G. Kogan, *Phys. Rev. Lett.* **70**, 2948 (1993).